

---

# CLUSTERING THE NEAREST NEIGHBOR GAUSSIAN PROCESS

---

A PREPRINT

 **Ashlynn Crisp**

Department of Mathematics and Statistics  
Portland State University  
Portland, OR  
acrisp@pdx.edu

 **Daniel Taylor-Rodríguez**

Department of Mathematics and Statistics  
Portland State University  
Portland, OR  
dantayrod@pdx.edu

 **Andrew O. Finley**

Department of Statistics and Probability  
Michigan State University  
East Lansing, MI  
finleya@msu.edu

January 22, 2025

## ABSTRACT

Gaussian processes are ubiquitous as the primary tool for modeling spatial data. However, the Gaussian process is limited by its  $\mathcal{O}(n^3)$  cost, making direct parameter fitting algorithms infeasible for the scale of modern data collection initiatives. The Nearest Neighbor Gaussian Process (NNGP) was introduced as a scalable approximation to dense Gaussian processes which has been successful for  $n \sim 10^6$  observations. This project introduces the *clustered Nearest Neighbor Gaussian Process* (cNNGP) which reduces the computational and storage cost of the NNGP. The accuracy of parameter estimation and reduction in computational and memory storage requirements are demonstrated with simulated data, where the cNNGP provided comparable inference to that obtained with the NNGP, in a fraction of the sampling time. To showcase the method’s performance, we modeled biomass over the state of Maine using data collected by the Global Ecosystem Dynamics Investigation (GEDI) to generate wall-to-wall predictions over the state. In 16% of the time, the cNNGP produced nearly indistinguishable inference and biomass prediction maps to those obtained with the NNGP.

**Keywords** Reduced order modeling, Gaussian spatial process, distance matrix clustering, biomass modeling, GEDI

## 1 Introduction

Gaussian processes (GPs) have been the customary approach for modeling spatial dependence in data. However, as modern datasets continue to grow increasingly large, fitting the original dense GP has become infeasible due to its  $\mathcal{O}(n^3)$  computational complexity. As a consequence, several approaches have been developed to approximate spatial processes.

Fixed rank [Cressie and Johannesson, 2008], lattice kriging [Nychka et al., 2015] and stochastic partial differential equations [Lindgren et al., 2011] assume the spatial process can be decomposed into a linear combination of basis functions. Spatial metakriging [Minsker et al., 2017] and spatial partitioning (e.g., Sang et al. [2011]) distribute computation by partitioning the data into subsets. Covariance tapering [Furrer et al., 2006] assumes pairs of locations with a sufficiently small covariance are independent, improving computational performance by creating a sparse covariance matrix. Banerjee et al. [2008] introduced predictive processes which use a set of “knots” as reference points to predict values at other locations. If the observations form a regular grid, periodic embedding [Guinness, 2019] uses discrete Fourier transforms, providing computational efficiency through fast Fourier transforms. Gapfill [Gerber et al., 2018] and the local approximate Gaussian process [Gramacy and Apley, 2015] use local subsets to make predictions.

Similarly to the Gapfill and local approximate GP methods, the Nearest Neighbor Gaussian Process (NNGP) [Datta et al., 2016] reduces computational cost by only considering neighboring locations. In a series of competitions between many of these approximation strategies, Heaton et al. [2019], Hong et al. [2023] found that the NNGP had competitive computational and predictive performance. Additionally, Finley et al. [2019] provided alternative formulations of the NNGP to further improve computational efficiency and convergence, while Guinness [2018] showed grouping calculations for observations can improve model accuracy.

More recently, Peruzzi et al. [2022] developed the Meshed Gaussian Process (MGP), which makes use of a directed acyclic graph over a tessellation of the spatial domain to induce a highly scalable dependence structure that enables investigating problems over very large spatial domains. Specifically, the graph uses the tessellation together with a relatively small set of *reference* locations to induce the dependence over the entire spatial domain, and renders the approach computationally scalable by assuming that locations in *non-reference* sets are independent, conditional on the reference sets. While the MGP constitutes an innovative and highly scalable approach, it has some limitations worth pointing out. Most importantly, the conditional independence assumption within and across partitions of non-reference sets can be restrictive and may lead to artifacts (e.g., boundary effects between partitions). Further, the quality of the model is strongly influenced by how the spatial domain is partitioned, making the approach sensitive to parameter tuning and potentially challenging to implement.

In this article we introduce the *clustered NNGP* (cNNGP), which offers comparable inferential performance to the NNGP while significantly reducing computational cost. The cNNGP saves computation and memory by identifying groups of locations whose nearest neighbor sets have similar distance patterns, and as such can be clustered together to reduce the number of operations required. One of the most computationally expensive pieces of fitting NNGP models is calculating kriging weights and the conditional variances to sample spatial random effects. As  $n$  grows to be in the order of millions of observations, the  $\mathcal{O}(nm^3)$  cost of an NNGP becomes substantial. Our proposed algorithm reduces this  $nm^3$  cost of the NNGP to  $\kappa m^3$ , where  $\kappa \ll n$ . Our cNNGP also reduces the storage requirements for model fitting. The number of required matrices in memory drops from  $n$  to  $\kappa$  so that the memory cost reduces from  $\mathcal{O}(nm^2)$  to  $\mathcal{O}(\kappa m^2)$ .

While conceptualized independently, our approach is similar in spirit to the *caching idea* introduced in Peruzzi et al. [2022] for the MGP, where by building the reference points on a regularly-spaced lattice, the covariances among reference points can be cached and reused. However, our approach enables sharing covariance information without requiring the locations to be built on a lattice and has a relatively straightforward implementation.

The code implementing the cNNGP, including the simulations presented below is available [here](#). Our implementation of the cNNGP uses source code from the *spNNGP* [Finley et al., 2022] and the *leaderCluster* [Arnold, 2023] R packages, with custom modifications to incorporate the proposed methods.

The remainder of this paper is organized as follows. In Section 2 we introduce the methods, first providing a brief overview of the NNGP, and then describing the cNNGP algorithm. In Section 3 we provide results from a simulation experiment on two datasets that are small enough to be able to compare the original NNGP with the proposed algorithm’s performance. Then, in Section 4 we use the proposed approach to model biomass estimates from the Global Ecosystem Dynamics Investigation (GED) [Dubayah et al., 2020]. Lastly, in Section 5 we conclude with a brief discussion of the cNNGP’s benefits and limitations.

## 2 Methods

In this section, we detail the methods underlying our approach, beginning with a brief overview of Gaussian Processes and their approximation through the NNGP, followed by a description of our novel modifications to the standard NNGP framework.

### 2.1 Background and Notation

A Gaussian process is defined as a stochastic process over a region  $\mathcal{D}$  such that the joint distribution of any finite collection of observations taken from locations in  $\mathcal{D}$  follow a multivariate normal distribution.

Let  $\mathbf{w}(\mathbf{s})$  denote a  $q$ -variate spatial random effect at location  $\mathbf{s} \in \mathcal{D}$ . Assuming a zero-centered GP,  $(\mathbf{w}(\mathbf{s}_1)', \mathbf{w}(\mathbf{s}_2)', \dots, \mathbf{w}(\mathbf{s}_n)')' \sim N(\mathbf{0}, \mathbf{C}_S(\boldsymbol{\theta}))$ , where  $S = \{\mathbf{s}_1, \dots, \mathbf{s}_n\} \in \mathcal{D}$  and  $\mathbf{C}_S(\boldsymbol{\theta})$  is the  $nq \times nq$  cross-covariance matrix with entries parameterized by  $\boldsymbol{\theta}$ .

GPs offer convenient marginal and conditional distributions for each  $\mathbf{w}(\mathbf{s}_i)$ . This is an important point to consider, in light of the fact that the joint distribution of an  $nq$ -dimensional vector  $\mathbf{w}_S$  can be written as the product of conditional

densities

$$p(\mathbf{w}_S) = p(\mathbf{w}(s_1)) p(\mathbf{w}(s_2)|\mathbf{w}(s_1)) \dots p(\mathbf{w}(s_n)|\mathbf{w}(s_{n-1}) \dots \mathbf{w}(s_1)). \quad (1)$$

Evaluating this product requires conditioning on sets up to size  $n - 1$ , which for large  $n$  implies a prohibitively costly computational burden. To overcome this limitation, Datta et al. [2016] developed the NNGP, which induces sparsity in the GP by assuming conditional independence of locations given their nearest neighbors, therefore drastically reducing the size of these conditioning sets. Note that, the joint density expressed by Equation 1 as a product of conditional densities, implies an ordering on the locations that defines the conditioning sets. Although this ordering has no relevance in the evaluation of the dense GP, as shown in Guinness [2018], the quality of the approximation provided by the NNGP is strongly influenced by how observations are ordered.

Here, we use the `order_maxmin_exact` function provided by the `GPvecchia` package in R [Katzfuss et al., 2024]. Once the points are ordered, the conditioning sets are replaced with smaller sets consisting of the nearest  $m$  neighbors of each location  $s$  measured by Euclidean distance. Let  $N(s_i) \in \{s_1, s_2, \dots, s_{i-1}\}$  be the set of  $m$  nearest neighbors of  $s_i$ . Then, Equation 1 can be approximated with:

$$\tilde{p}(\mathbf{w}_S) = \prod_{i=1}^n p(\mathbf{w}(s_i)|\mathbf{w}_{N(s_i)}). \quad (2)$$

Let  $\mathbf{C}_{s, N(s)}$  be the covariance matrix between  $s$  and its neighbor set and  $\mathbf{C}_{N(s)}$  be the covariance matrix of  $N(s)$ . Equation (2) implies conditional independence across locations given its nearest neighbors, with the conditional density for  $\mathbf{w}(s)|\mathbf{w}_{N(s)}$  given by

$$\mathbf{w}(s)|\mathbf{w}_{N(s)} \sim N(\mathbf{B}_s \mathbf{w}_{N(s)}, \mathbf{F}_s), \quad (3)$$

with  $\mathbf{B}_s = \mathbf{C}_{s, N(s)} \mathbf{C}_{N(s)}^{-1}$  and  $\mathbf{F}_s = \mathbf{C}_s - \mathbf{C}_{s, N(s)} \mathbf{C}_{N(s)}^{-1} \mathbf{C}_{N(s), s}$  as derived in Datta et al. [2016]. Hence, the approximated joint density is

$$\tilde{p}(\mathbf{w}_S) = \prod_{i=1}^n N(\mathbf{w}(s_i)|\mathbf{B}_{s_i} \mathbf{w}_{N(s_i)}, \mathbf{F}_{s_i}). \quad (4)$$

Using this approximation to the Gaussian Process, the NNGP can model the spatially-correlated errors in a regression model, that is,

$$\mathbf{y}(s) = \mathbf{X}(s)' \boldsymbol{\beta} + \mathbf{Z}(s)' \mathbf{w}(s) + \boldsymbol{\epsilon}(s), \quad (5)$$

where  $s \in \mathcal{D}$ ,  $\mathbf{y}(s)$  is the  $l$ -variate response. Letting  $p = \sum_{k=1}^l p_k$ ,  $\boldsymbol{\beta}$  is the  $p$ -dimensional vector of regression coefficients for the fixed  $l \times p$  block-diagonal matrix of spatially referenced predictors  $\mathbf{X}(s)'$ . Additionally,  $\mathbf{Z}(s)'$  is the  $l \times q$  design matrix for the spatial process  $\mathbf{w}(s)$  (in our subsequent analyses we have  $l = q$  and set  $\mathbf{Z}(s)' = \mathbf{I}_l$ ), and  $\boldsymbol{\epsilon}(s) \stackrel{\text{iid}}{\sim} N(\mathbf{0}, \text{diag}(\tau_1^2, \dots, \tau_l^2))$  is the  $l \times 1$  uncorrelated error term.

## 2.2 Clustered Nearest Neighbor Gaussian Process

The clustered NNGP speeds up computation by identifying approximately recurring spatial patterns in the coordinates of the data and reducing the number of computations associated with these recurring patterns. For a location  $s$ , the estimate of  $\mathbf{w}(s)$  depends on the covariance between  $\mathbf{w}(s)$  and  $\mathbf{w}_{N(s)}$ . This covariance depends on the distances between  $s$  and  $N(s)$  as well as the pairwise distances in the neighbor set  $N(s)$ . Under stationarity and isotropy, if two points have similar distances to their neighbor sets and similar pairwise distances within their neighbor sets, then their covariance to/within their neighbor sets will also be approximately the same, assuming the same parameters for the covariance function. More formally, let  $N_s^* = \{s\} \cup N(s)$  and  $\mathbf{D}_s^*$  be the  $(m+1) \times (m+1)$  distance matrix between locations in  $N_s^*$ , note that the matrices  $\mathbf{B}_s$  and  $\mathbf{F}_s$  are computed using only  $\mathbf{D}_s^*$  and the vector of covariance parameters  $\boldsymbol{\theta}$ . This means that, for a particular  $\boldsymbol{\theta}$ , if two locations  $s, r \in \mathcal{S}$  have the same distance matrices such that  $\mathbf{D}_s^* = \mathbf{D}_r^*$ , then:

$$\mathbf{C}_s^* = \mathbf{C}_r^* \Rightarrow \begin{cases} \mathbf{B}_s = \mathbf{B}_r \\ \mathbf{F}_s = \mathbf{F}_r \end{cases}.$$

This is the idea behind the clustered Nearest Neighbor Gaussian Process. If two points have similar distance matrices, then their  $\mathbf{B}$  and  $\mathbf{F}$  matrices will also be similar given the same values of  $\boldsymbol{\theta}$ . Taking advantage of similar distance matrices in the data reduces the number of inverses required and the number of covariance matrices needed in memory.

In the cNNGP, there is first a preprocessing step to find locations which have similar distance matrices. Denote by  $\mathbf{d}_s$  the vector containing the values inside of the lower triangle of  $\mathbf{D}_s^*$ , such that  $\mathbf{d}_s$  is the  $\binom{m+1}{2}$  vector of unique distances among locations in  $N_s^*$ . Recall that  $\mathbf{D}_s^*$  is the pairwise distance matrix between locations in  $N_s^* = \{s\} \cup N(s)$ , where  $N(s)$  is the neighbor set of  $s$  ordered from closest to farthest neighbor, so that the  $\mathbf{D}_s^*$  for all  $s$  matrices are ordered the same for each point. To find locations in  $\mathcal{S}$  which have similar distance matrices,  $\mathbf{d}_s$  is extracted for each location and assigned to groups using a clustering algorithm. Note that the first  $m$  locations will not be considered for this preprocessing step since these locations will have fewer than  $m$  neighbors (as such, each will be its own cluster); after the first  $m$  locations, the distance matrices will have the same dimensions.

We use Hartigan’s leader algorithm [Hartigan, 1975] for clustering since it provides an upper bound for the approximation error of  $\mathbf{D}_s^*$  and it easily scales up to a massive number of observations. To elaborate, the clustering algorithm takes a radius value  $r$ . It then iterates through each  $\mathbf{d}_{s_i}$  for  $i = 1, \dots, n$  as follows:  $\mathbf{d}_{s_1}$  is set as the cluster leader for cluster 1. If  $\|\mathbf{d}_{s_2} - \mathbf{d}_{s_1}\| > r$ , then  $\mathbf{d}_{s_2}$  becomes the cluster leader for cluster 2, else it joins cluster 1. Similarly, the distance between  $\mathbf{d}_{s_3}$  and the previous clusters is computed. If  $\mathbf{d}_{s_3}$  is within the radius of a previous cluster, it is assigned to that cluster, otherwise it becomes a cluster leader. This continues for all  $i = 4, \dots, n$ , resulting in  $\kappa$  groups of distance matrices all within distance  $r$  to their cluster leaders.

We set  $r$  by computing the corresponding  $\kappa$  value for several values of  $r$  and choose the  $r$  value where the changes in  $\kappa$  start to diminish. For large datasets, we recommend using the principal components of the  $\binom{m+1}{2}$  columns of the matrix of neighbor set distances given by  $(\mathbf{d}_{s_1}, \dots, \mathbf{d}_{s_n})'$  in the clustering to reduce the dimensionality of the vectors being clustered. We used the principal components which captured 90% of the variance in the  $(\mathbf{d}_{s_1}, \dots, \mathbf{d}_{s_n})'$  matrix.

Let  $\bar{\mathbf{D}}_\ell$  ( $\ell = 1, \dots, \kappa \ll n$ ) be the mean cluster distance matrix for all locations assigned to cluster  $\ell$ , and  $\bar{\mathbf{C}}^\ell$  be the covariance matrix between the point and its  $m$  neighbors, which depends on  $\bar{\mathbf{D}}_\ell$  and  $\boldsymbol{\theta}$ . Although  $\bar{\mathbf{D}}_\ell$  remains fixed (since clusters are precalculated), at every iteration of the MCMC algorithm a new value for  $\boldsymbol{\theta}$  is sampled, so  $\bar{\mathbf{C}}^\ell$  must be updated with a new  $\boldsymbol{\theta}$  at each iteration. Let  $\bar{\mathbf{C}}_{\{1\}, \setminus \{1\}}^\ell$  denote the first row of  $\bar{\mathbf{C}}^\ell$  excluding the first position. With this notation, compute

$$\begin{aligned}\bar{\mathbf{B}}_\ell &= \bar{\mathbf{C}}_{\{1\}, \setminus \{1\}}^\ell \left( \bar{\mathbf{C}}_{\setminus \{1\}, \setminus \{1\}}^\ell \right)^{-1}, \\ \bar{\mathbf{F}}_\ell &= \bar{\mathbf{C}}_{\{1\}, \{1\}}^\ell - \mathbf{B}'_\ell \bar{\mathbf{C}}_{\setminus \{1\}, \{1\}}^\ell.\end{aligned}$$

Let  $\ell(s)$  denote the cluster to which the point  $s$  is assigned. The cNNGP approximation of the joint density  $\tilde{p}(\mathbf{w}_S)$  is

$$\tilde{p}(\mathbf{w}_S) = \prod_{i=1}^n N(\mathbf{w}(s_i) | \bar{\mathbf{B}}_{\ell(s_i)} \mathbf{w}_{N(s_i)}, \bar{\mathbf{F}}_{\ell(s_i)}). \quad (6)$$

Once the posterior samples for the model are obtained, predictions  $\mathbf{y}^*(\mathbf{t})$  are obtained from the posterior predictive distribution of  $\mathbf{y}(\mathbf{t}) | \mathbf{y}$ , where  $\mathbf{y} = (\mathbf{y}(s_1)', \mathbf{y}(s_2)', \dots, \mathbf{y}(s_n)')$ , is carried out for a location  $\mathbf{t}$  by sampling  $N(\mathbf{X}(\mathbf{t})' \boldsymbol{\beta} + \mathbf{Z}(\mathbf{t})' \mathbf{w}(\mathbf{t}), \boldsymbol{\Psi})$ , where  $\boldsymbol{\Psi} = \text{diag}(\tau_1^2, \dots, \tau_l^2)$ , if  $\mathbf{t}$  was included in the model fitting. If  $\mathbf{t}$  is a new point, then samples of  $\mathbf{w}^*(\mathbf{t})$  must be generated from  $N(\mathbf{B}_t \mathbf{w}_S, \mathbf{F}_t)$  first, and then posterior samples for  $\mathbf{y}^*(\mathbf{t})$  can be drawn from  $N(\mathbf{X}(\mathbf{t})' \boldsymbol{\beta} + \mathbf{Z}(\mathbf{t})' \mathbf{w}^*(\mathbf{t}), \boldsymbol{\Psi})$ .

### 3 Simulation Experiments

In order to compare the performance of the cNNGP to the NNGP, we generated simulated datasets so that the true values of the parameters are known. This allows comparisons for the estimates of parameters and coverage probabilities for the 95% credible intervals. After assessing the quality of the approximation provided by the cNNGP, we measure the gains in computational efficiency with respect to the NNGP. The sampling time is reported as the “user” time measured by the R function *proc.time*, and every model was fit with OpenMP support with 3 threads.

#### 3.1 Experiment Setup

We generated two datasets, one with  $n = 1,000$  and another one with  $n = 10,000$  locations assuming a univariate response ( $l = 1$ ) and univariate spatial process ( $q = 1$ ). The coordinates were drawn from a unit square domain. The model has  $p = 2$ , so that there is an intercept and one covariate drawn from a standard normal distribution. We used the exponential covariance function:

$$C(\mathbf{s}_i, \mathbf{s}_j; \phi, \sigma^2) = \sigma^2 e^{-\phi \|\mathbf{s}_i - \mathbf{s}_j\|},$$

where  $\|\cdot\|$  is the Euclidean norm. Following the work of Datta et al. [2016], the values to generate the data were 12 and 1 for  $\phi$  and  $\sigma^2$ , respectively. The  $\beta$  parameters were set at 1 and 5 for  $\beta_0$  and  $\beta_1$ . The variance for  $\epsilon$  was  $\tau^2 = 0.1$ . The priors given to each parameter were: Uniform(3,30) for  $\phi$ , InverseGamma(2,1) for  $\sigma^2$ , InverseGamma(2,0.1) for  $\tau^2$ , and a flat prior for  $\beta$ . The number of neighbors  $m$  was set at 20 for each model.

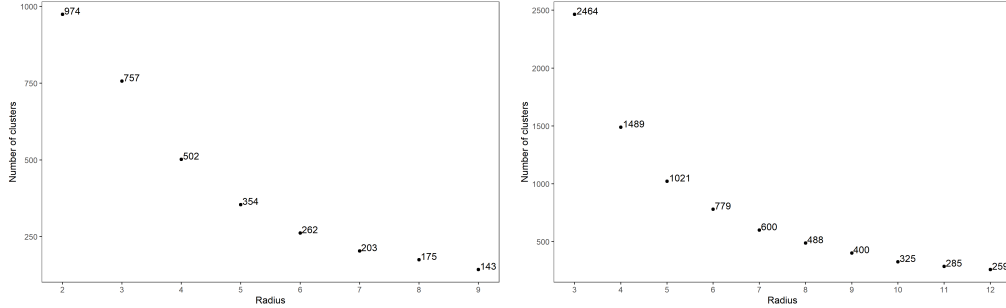


Figure 1: Number of clusters  $\kappa$  versus clustering radius  $r$ . **(Left):** figure shows results for 1,000 point dataset. **(Right):** figure shows results for 10,000 point dataset. The value of  $r$  was set at 6 and 7 for the model fitting for the 1,000 point and 10,000 point datasets, respectively.

Clusters for each dataset were based on the principal components computed using their respective distance matrices. The values for the clustering radius  $r$  were set at 6 and 7 for  $n = 1,000$  and  $n = 10,000$ , respectively (Figure 1). Each model was run for 20,000 iterations, with the first 7,500 iterations discarded as burn-in. Each sampler was initialized at the same values. The regression coefficients were initialized at their ordinary least squares estimates  $\hat{\beta}_{OLS}$ ,  $\phi$  was initialized at the mean of its prior distribution, and  $\sigma^2$  and  $\tau^2$  were each initialized at  $\frac{1}{2}\text{Var}(\mathbf{y} - \mathbf{X}\hat{\beta}_{OLS})$ , where  $\mathbf{y}$  is the vector of responses and  $\mathbf{X}$  is the corresponding design matrix. All models showed quick convergence and similar behavior in the traceplots.

### 3.2 Parameter Estimation Results

For both datasets, the cNNGP provided similar parameter estimates and intervals to those obtained with the NNGP. Table 1 shows the comparison of the parameter posterior credible intervals and point estimates (posterior means) for both models.

	True	1,000 locations		10,000 locations	
		cNNGP	NNGP	cNNGP	NNGP
$\beta_1$	1.00	0.77 (0.53, 1)	0.78 (0.57, 1)	1.11 (1, 1.19)	1.13 (1.04, 1.22)
$\beta_2$	5.00	5.03 (4.99, 5.07)	5.02 (4.99, 5.06)	5 (4.99, 5.01)	5 (4.99, 5.01)
$\sigma^2$	1.00	0.8 (0.67, 0.96)	0.86 (0.72, 1.02)	0.85 (0.7, 1.1)	0.98 (0.79, 1.26)
$\tau^2$	0.10	0.05 (0.02, 0.11)	0.04 (0.02, 0.08)	0.08 (0.07, 0.09)	0.1 (0.1, 0.11)
$\phi$	12.00	18.21 (13.71, 22.48)	20.96 (16.19, 25.45)	13.91 (10.11, 17.02)	12.72 (9.54, 15.84)

Table 1: Posterior mean and 95% credible intervals for parameter estimates from the cNNGP and NNGP for the simulated datasets.

For example, the cNNGP captured the true value of  $\tau^2$  in its posterior credible interval while the NNGP did not on the smaller dataset. However, this trend is reversed in the larger dataset. Similarly, the cNNGP gave a closer point estimate for  $\phi$  in the smaller dataset but not for the larger dataset. More often than not, the cNNGP gave slightly wider credible interval estimates for the parameters than the NNGP, although there were some differences these were overall relatively minor.

The coverage probability for  $w$  for the cNNGP (NNGP) was 81.5% (78.5%) and 91.4% (91.5%) for  $n = 1,000$  and  $n = 10,000$ , respectively. The credible interval widths were also similar between the two models, see Figure 2. The median interval widths for the cNNGP (NNGP) was 0.967 (0.876) and 0.894 (0.887) for  $n = 1,000$  and  $n = 10,000$ , respectively, indicating that the cNNGP provides similar coverage probabilities for  $w$  while achieving competitively narrow credible intervals to those obtained with the full NNGP. A comparison between the posterior samples for  $w$  from each model is included in Figure 3, where the 2.5th, 50th, and 97.5th quantiles of the difference between the

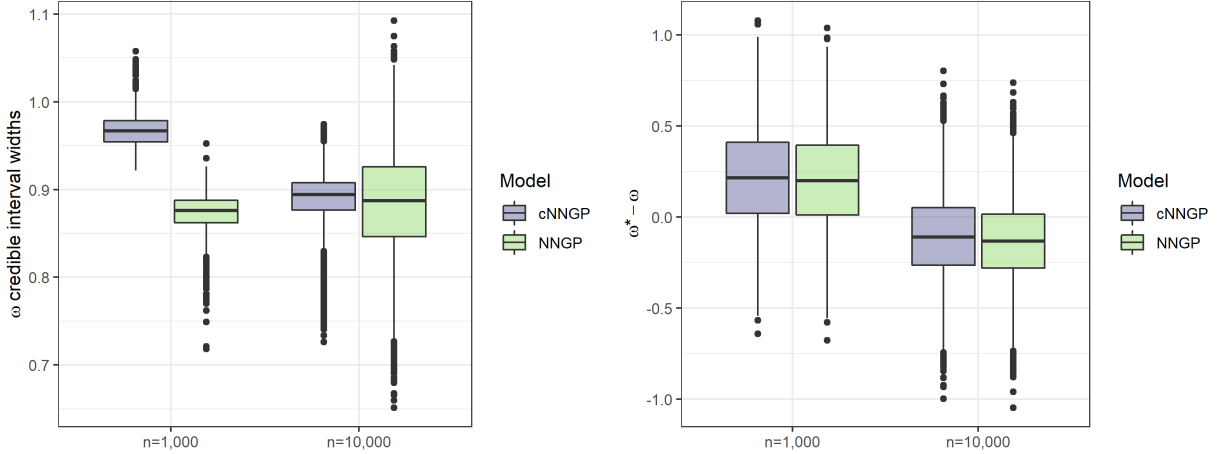


Figure 2: Analysis of spatial effect  $w$ . **(Left)**: Posterior 95% credible interval widths for  $w$  from simulated datasets. **(Right)**: Error in estimates  $w^*$  for  $w$  calculated as  $w^* - w$ .

posterior samples and the true values for the spatial effects are displayed by column and the rows show the results for either the cNNGP or the NNGP.

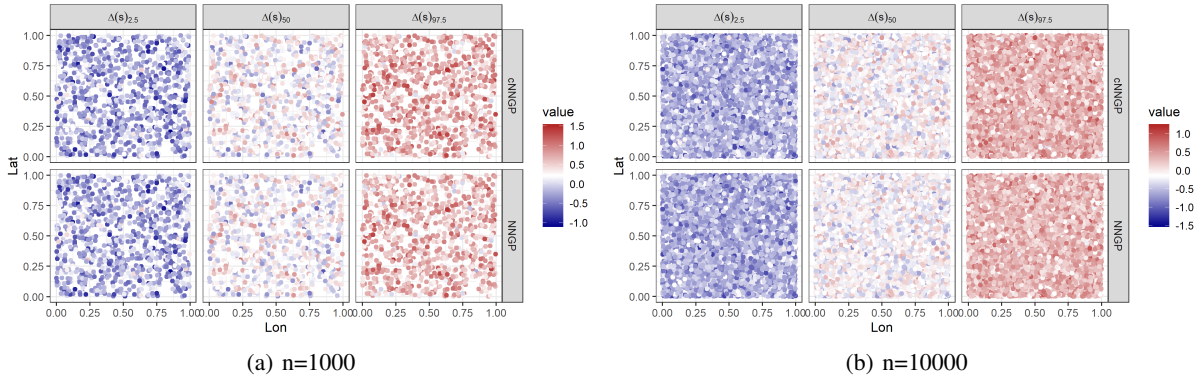


Figure 3: Posterior samples for  $w^*(s)$  minus true spatial effect  $w(s)$ ,  $\Delta(s) = w^*(s) - w(s)$ . The 2.5, 50, and 97.5 percentiles of  $\Delta(s)$  are shown in each column as  $\Delta(s)_{2.5}$ ,  $\Delta(s)_{50}$ , and  $\Delta(s)_{97.5}$ , respectively.

As is the case with the spatial effects, the performance of both models for the response variable  $y$ , the cNNGP provides slightly wider credible intervals, resulting in higher coverage probabilities for  $y$  (Figure A1). The coverage probability for  $y$  was 100% for the small dataset for both models. For  $n = 10,000$ , the cNNGP obtained 98.7% coverage while the NNGP had 93.7%. Interestingly, the difference between the predicted  $y^*$  and true response  $y$ , i.e.,  $y^* - y$ , is very similar between the two models. For these simulated datasets, the cNNGP increased the uncertainty bounds on  $y$  to capture more of the responses in their credible intervals while attaining point estimates comparable to those from the NNGP.

Figure 4 shows the sampling duration and number of  $m \times m$  matrices required for each dataset and model. The sampling times in seconds for the cNNGP (NNGP) on the 1,000-location and 10,000-location datasets were 197 (570) and 938 (7,080), respectively. This means the cNNGP took 35% and 13% of the time taken by the full NNGP for the small and large dataset. This reduction in computation time for larger  $n$  is due to the larger reduction in required matrix storage and inversions. The cNNGP required 262 (27%) and 600 (6%) of the full  $20 \times 20$  distance matrices compared to 980 and 9,980 using the full NNGP.

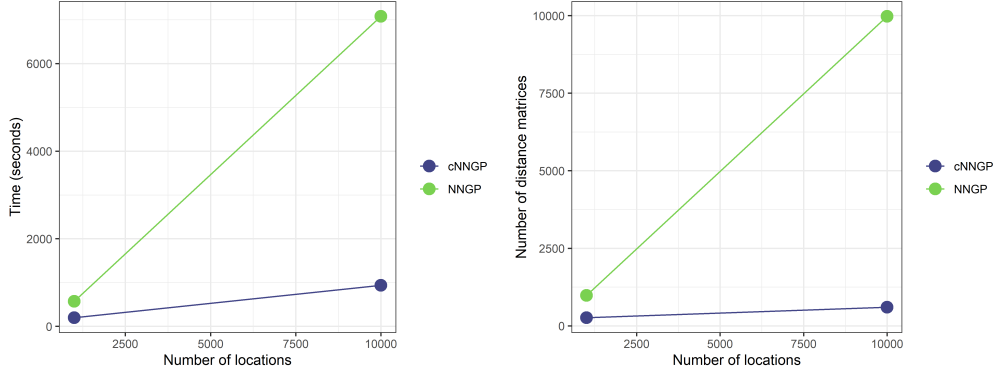


Figure 4: Simulated dataset sampling time and matrix storage requirements: **(Left)**: MCMC sampling time in seconds for the cNNGP and NNGP models on each simulated dataset. **(Right)**: Number of  $m \times m$  distance matrices  $\kappa$  required for each model on each dataset.

#### 4 Application: Biomass Prediction using GEDI Data

The GEDI project captures 3D structures of Earth to help understand the Earth’s carbon cycle by measuring forest canopy heights and biomass. The GEDI instrument is a geodetic-class, light detection and ranging (lidar) laser system. It was installed onboard the International Space Station (ISS) in 2018 to sample about 4% of the Earth’s land surface between  $51.6^\circ$  N & S latitude at a 25 m footprint resolution [Dubayah et al., 2020]. We use the GEDI L4B data product which contains global mean aboveground biomass density estimates between  $52^\circ$  N & S latitude at a 1 km by 1 km resolution, collected between April 18th, 2019 to March 16th, 2023. GEDI collects data along the ISS’s orbital path, hence, at higher Earth latitudes, these paths do not yield complete data coverage as shown in Figure 5. Our goal is to complete the L4B coverage using cNNGP to predict for missing data and produce wall-to-wall forest biomass estimates over the state of Maine. In addition to borrowing information from observed GEDI pixels via spatial random effects, we use a complete-coverage tree canopy cover (TCC) dataset as a covariate [Housman et al., 2023]. The data used in this analysis are shown in Figure 5.

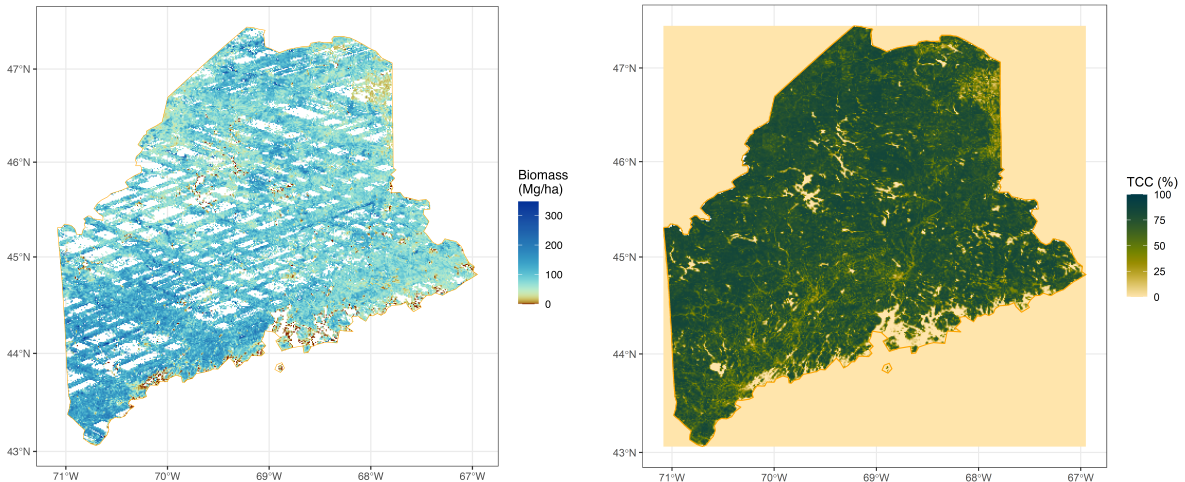


Figure 5: GEDI data for state of Maine. **(Left)**: Average above ground biomass from GEDI data. **(Right)**: Proportion of tree canopy cover.

At the 1 km by 1 km resolution, there are 86,949 pixels in Maine. We removed any values of TCC over 100%, leaving 86,802 pixels. Of these 16,914 pixels did not have recorded biomass values, and we deleted 112 values of biomass that were unrealistically high for Maine. Pixel centroids were used to compute distances in subsequent models. To form hold outs for comparing prediction performance, a 50 by 50 square grid was placed over Maine. Of these grid cells,

Parameter	cNNGP	NNGP
Intercept	25.29 (23.49, 27.28)	25.51 (23.7, 27.48)
TCC	0.97 (0.96, 0.99)	0.97 (0.95, 0.98)
$\sigma^2$	845.44 (813.59, 880.24)	893.62 (858.8, 931.13)
$\tau^2$	365.95 (353.75, 377.87)	364.23 (352.06, 376.03)
$\phi$	0.26 (0.24, 0.27)	0.27 (0.25, 0.28)

Table 2: Posterior mean and credible intervals for the GEDI data from the cNNGP and NNGP.

10% were sampled to be set aside for prediction, see Figure A3. This held out 6,851 pixels from the model fitting. The final counts were 62,925 pixels used for fitting, 6,851 known biomass values held out for prediction, and 17,026 pixels with missing biomass.

To determine the clustering radius, we first computed the principal components of the distance matrices. We retained only the components that explained 90% of the original variance and selected a sample of 10,000 locations. This approach allowed us to efficiently test the clustering procedure across multiple radius values, ultimately identifying a suitable radius for clustering the entire dataset. As before, we found the elbow of the graph of the number of clusters versus clustering radius, see Figure A2. Once  $r$  was set to 4 from the subsample, all the observations were clustered using  $r = 4$ , which provided for the full set of locations 4,168 clusters (i.e., unique distance matrices) to be used in model fitting, corresponding to 6.6% of the number of matrices used with the full NNGP.

The coordinates were scaled accordingly to have distances be measured in kilometers. For choosing the prior for  $\phi$ , 10,000 locations were subsampled and the minimum  $d_{min}$  and maximum  $d_{max}$  distances in this scaled subset of 10,000 locations were used to assign a uniform prior with lower bound  $3/d_{max}$  and upper bound  $3/d_{min}$ , resulting in a Uniform(0.01,3) prior. Flat priors were set for the intercept and TCC regression parameters. The priors for  $\sigma^2$  and  $\tau^2$  were chosen to be InverseGamma(2,600), where the hyperparameter values were selected to conform to the scale of the response. The chains were initialized following the same approach as the one used with the simulated data.

Each model was run for 10,000 MCMC iterations, and the chains for both models used the same seed and were initialized with the same values. The sampling time in seconds for the cNNGP was 3,161 and for the NNGP was 20,100. That is, the cNNGP took 16% of the time taken by the NNGP.

Table 2 shows that the credible interval bounds and posterior means for most parameters are quite similar between the cNNGP and the NNGP, with some differences in  $\sigma^2$ , the variance of the spatial process, where the estimates differ by about 5.4%. The maps of the predicted biomass values and standard error of the estimates are nearly indistinguishable between the two models (Figure 6).

The coverage probability for the predicted biomass holdout values from the cNNGP model was 94.9%, which was extremely close to the 95.3% coverage from the NNGP Figure A5. The median biomass credible interval widths on the holdout set for the cNNGP and NNGP were 114.7 and 117.4 respectively, meaning that the uncertainty in the predicted biomass values is comparable between models, as seen in Figure A4.

## 5 Discussion

The NNGP is a competitive approximation method for dense GPs over large datasets. However, NNGPs have  $\mathcal{O}(nm^3)$  complexity, which might preclude scaling as datasets increase to truly massive sizes. We proposed the clustered NNGP algorithm as an approximation to the NNGP which reduces computational cost by exploiting similar spatial patterns in the data among neighbor sets. Here, we compared the performance of the cNNGP and NNGP for simulated datasets with 1,000 and 10,000 locations, and used the methods to model GEDI biomass data.

In the simulated datasets, the cNNGP provided an excellent approximation in both datasets, estimating similar credible intervals and posterior means for the  $\theta$ ,  $\beta$ , and  $\epsilon$  parameters compared to the full NNGP. For the spatial effect  $w$ , the models provided similar coverage probabilities and estimated similar credible interval widths, especially for the larger dataset. This level of approximation required 35% (13%) of the time and 27% (6%) of the matrices compared to the NNGP for  $n = 1,000$  ( $n = 10,000$ ).

For the GEDI data, the cNNGP offered model parameter estimates comparable to those produced using the NNGP. The coverage probability for on a holdout dataset for the cNNGP at 94.9% and the NNGP had 95.3%. Additionally, the biomass credible intervals were not significantly larger than those from the NNGP. This approximation was fit using only 16% of the time needed for the full NNGP.

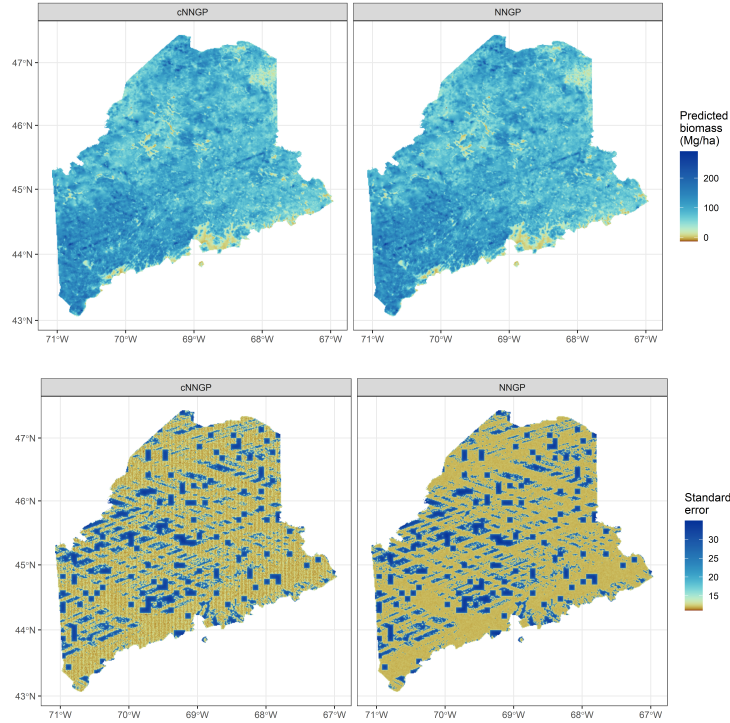


Figure 6: **(Top)**: Predicted biomass values for all GEDI locations. **(Bottom)**: Standard error of predicted biomass values.

Overall, we observed that the proposed approach leads to a drastic reduction in the sampling time for model fitting due to the clustering-based reduction. If the number of clusters  $\kappa$  is relatively small when compared to  $n$ , then there is a significant model fitting cost reduction from  $\mathcal{O}(nm^3)$  to  $\mathcal{O}(\kappa m^3)$ . Importantly,  $\kappa$  will vary based on the spatial patterns in the observations and the desired error tolerance. While the GEDI data was over 6 times larger than the 10,000-location simulated dataset, the reduction in sampling time was only 6 times faster than the full NNGP, compared to 7 times faster on the 10,000-location dataset due to the differences in spatial patterns.

It is important to note that in its current form the cNNGP only applies to stationary and isotropic spatial processes. The cNNGP reduces computational and storage costs by grouping similar covariance matrices, and this grouping step requires both conditions be met. Finally, the cNNGP is an approximation to the NNGP and is therefore limited to spatial processes where the NNGP is an appropriate model choice.

## Acknowledgements

This work was partially supported by the U.S. Department of Energy, Office of Science, Office of Advanced Scientific Computing Research Award DOE CSGF DE-SC0023112, the United States Forest Service, the National Science Foundation Awards RTG DMS-2136228 and DEB-2213565, and the National Aeronautics and Space Administration Carbon Monitoring system grants Hayes 2020 and 2023.

## References

- Noel Cressie and Gardar Johannesson. Fixed rank kriging for very large spatial data sets. *Journal of the Royal Statistical Society: Series B (Statistical Methodology)*, 70(1):209–226, 2008.
- Douglas Nychka, Soutir Bandyopadhyay, Dorit Hammerling, Finn Lindgren, and Stephan Sain. A multiresolution gaussian process model for the analysis of large spatial datasets. *Journal of Computational and Graphical Statistics*, 24(2):579–599, 2015.

- Finn Lindgren, Håvard Rue, and Johan Lindström. An explicit link between gaussian fields and gaussian markov random fields: the stochastic partial differential equation approach. *Journal of the Royal Statistical Society: Series B (Statistical Methodology)*, 73(4):423–498, 2011.
- Stanislav Minsker, Sanvesh Srivastava, Lizhen Lin, and David B Dunson. Robust and scalable bayes via a median of subset posterior measures. *The Journal of Machine Learning Research*, 18(1):4488–4527, 2017.
- Huiyan Sang, Mikyoung Jun, and Jianhua Z Huang. Covariance approximation for large multivariate spatial data sets with an application to multiple climate model errors. *The Annals of Applied Statistics*, pages 2519–2548, 2011.
- Reinhard Furrer, Marc G Genton, and Douglas Nychka. Covariance tapering for interpolation of large spatial datasets. *Journal of Computational and Graphical Statistics*, 15(3):502–523, 2006.
- Sudipto Banerjee, Alan E Gelfand, Andrew O Finley, and Huiyan Sang. Gaussian predictive process models for large spatial data sets. *Journal of the Royal Statistical Society: Series B (Statistical Methodology)*, 70(4):825–848, 2008.
- Joseph Guinness. Spectral density estimation for random fields via periodic embeddings. *Biometrika*, 106(2):267–286, 2019.
- Florian Gerber, Rogier de Jong, Michael E Schaepman, Gabriela Schaepman-Strub, and Reinhard Furrer. Predicting missing values in spatio-temporal remote sensing data. *IEEE Transactions on Geoscience and Remote Sensing*, 56(5):2841–2853, 2018.
- Robert B Gramacy and Daniel W Apley. Local gaussian process approximation for large computer experiments. *Journal of Computational and Graphical Statistics*, 24(2):561–578, 2015.
- Abhirup Datta, Sudipto Banerjee, Andrew O Finley, and Alan E Gelfand. Hierarchical nearest-neighbor gaussian process models for large geostatistical datasets. *Journal of the American Statistical Association*, 111(514):800–812, 2016.
- Matthew J Heaton, Abhirup Datta, Andrew O Finley, Reinhard Furrer, Joseph Guinness, Rajarshi Guhaniyogi, Florian Gerber, Robert B Gramacy, Dorit Hammerling, Matthias Katzfuss, et al. A case study competition among methods for analyzing large spatial data. *Journal of Agricultural, Biological and Environmental Statistics*, 24:398–425, 2019.
- Yiping Hong, Yan Song, Sameh Abdulah, Ying Sun, Hatem Ltaief, David E. Keyes, and Marc G. Genton. The third competition on spatial statistics for large datasets. *Journal of Agricultural, Biological and Environmental Statistics*, 28(4):618–635, 2023.
- Andrew O Finley, Abhirup Datta, Bruce D Cook, Douglas C Morton, Hans E Andersen, and Sudipto Banerjee. Efficient algorithms for bayesian nearest neighbor gaussian processes. *Journal of Computational and Graphical Statistics*, 28(2):401–414, 2019.
- Joseph Guinness. Permutation and grouping methods for sharpening gaussian process approximations. *Technometrics*, 60(4):415–429, 2018.
- Michele Peruzzi, Sudipto Banerjee, and Andrew O Finley. Highly scalable bayesian geostatistical modeling via meshed gaussian processes on partitioned domains. *Journal of the American Statistical Association*, 117(538):969–982, 2022.
- Andrew O. Finley, Abhirup Datta, and Sudipto Banerjee. spNNGP R package for nearest neighbor Gaussian process models. *Journal of Statistical Software*, 103(5):1–40, 2022. doi:10.18637/jss.v103.i05.
- Taylor B. Arnold. *leaderCluster: Leader Clustering Algorithm*, 2023. URL <https://CRAN.R-project.org/package=leaderCluster>. R package version 1.5.
- Ralph Dubayah, James Bryan Blair, Scott Goetz, Lola Fatoyinbo, Matthew Hansen, Sean Healey, Michelle Hofton, George Hurtt, James Kellner, Scott Luthcke, et al. The global ecosystem dynamics investigation: High-resolution laser ranging of the earth’s forests and topography. *Science of remote sensing*, 1:100002, 2020.
- Matthias Katzfuss, Marcin Jurek, Daniel Zilber, and Wenlong Gong. *GPvecchia: Scalable Gaussian-Process Approximations*, 2024. URL <https://CRAN.R-project.org/package=GPvecchia>. R package version 0.1.7.
- John A. Hartigan. *Clustering Algorithms*, chapter 3. John Wiley & Sons, Inc., USA, 99th edition, 1975. ISBN 047135645X.
- Ian Housman, Karen Schleeweis, Josh Heyer, Bonnie Rufenacht, Stacie Bender, Kevin Megown, Wendy Goetz, and Seth Bogle. National land cover database tree canopy cover methods v2021.4. GTAC-10268-RPT1. Salt Lake City, UT: U.S. Department of Agriculture, Forest Service, Geospatial Technology and Applications Center, 2023.

## 6 Appendix

The appendix includes one additional figure from the analysis of the simulated data sets, and four figures for the GEDI data analysis.

### 6.1 Additional figures from simulations

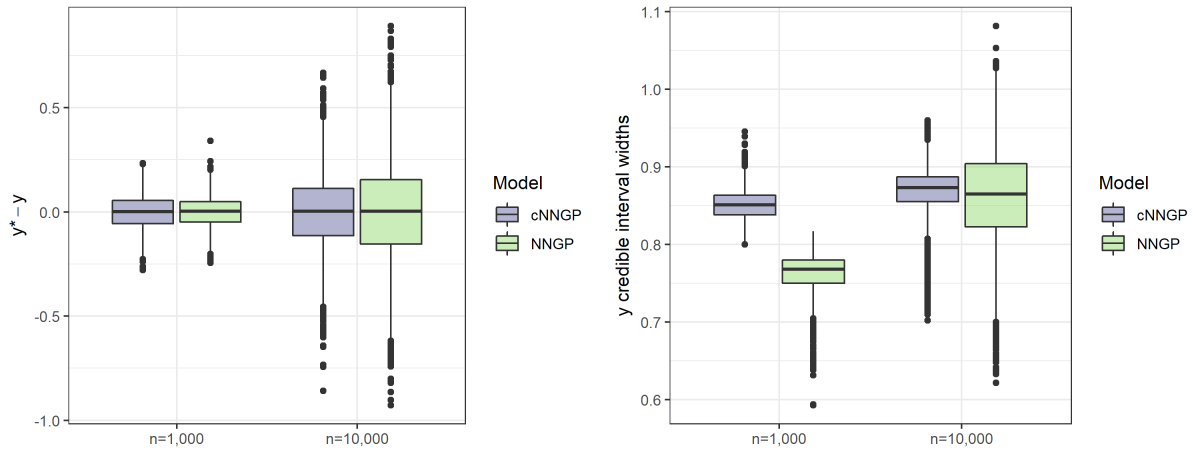


Figure A1: Analysis of response variable  $y$ . **(Left):** Error in response estimate  $y^*$ . Boxplots show difference between posterior estimate and true value  $y^* - y$ . **(Right):** Posterior credible interval widths for response value  $y^*$ .

### 6.2 Additional figures GEDI data analysis

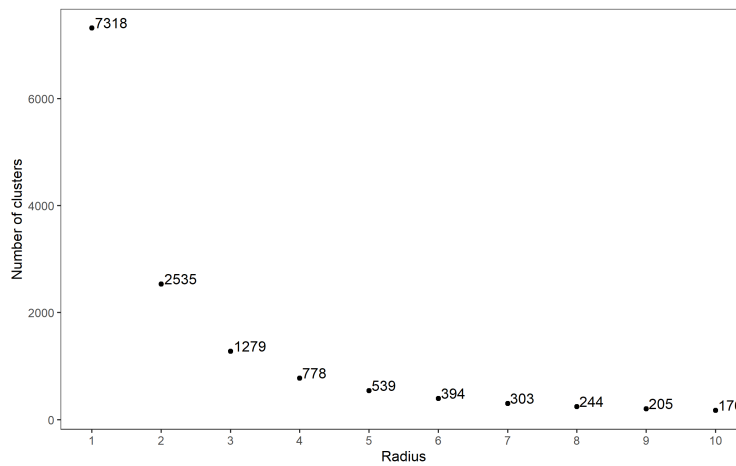


Figure A2: Number of clusters vs. clustering radius for GEDI data. The radius value of 4 was selected for the analysis.

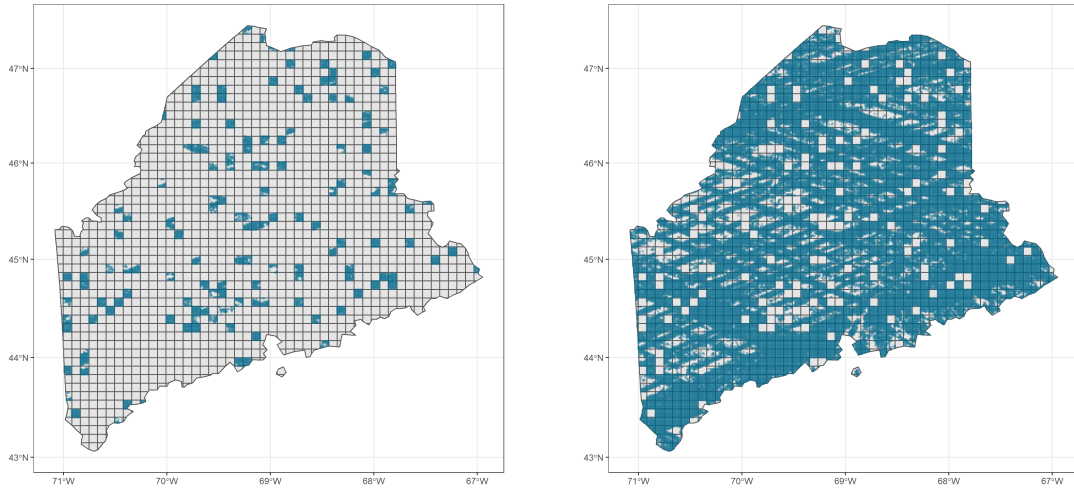


Figure A3: **(Left)**: GEDI data withheld for prediction. **(Right)**: GEDI data used for model fitting.

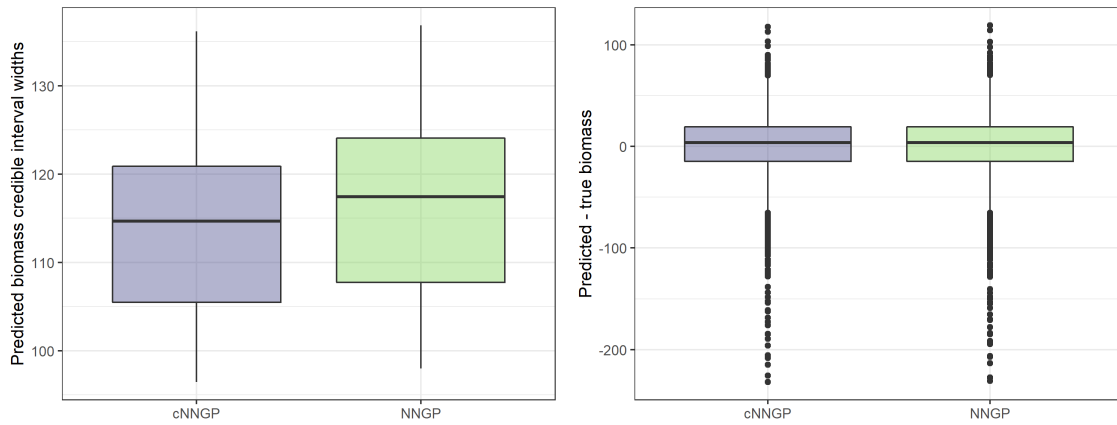


Figure A4: Model comparison for GEDI holdout data. **(Left)**: Predicted biomass credible interval widths for cNNGP and NNGP. **(Right)**: Error in biomass estimates calculated as predicted (posterior mean) minus true biomass values.

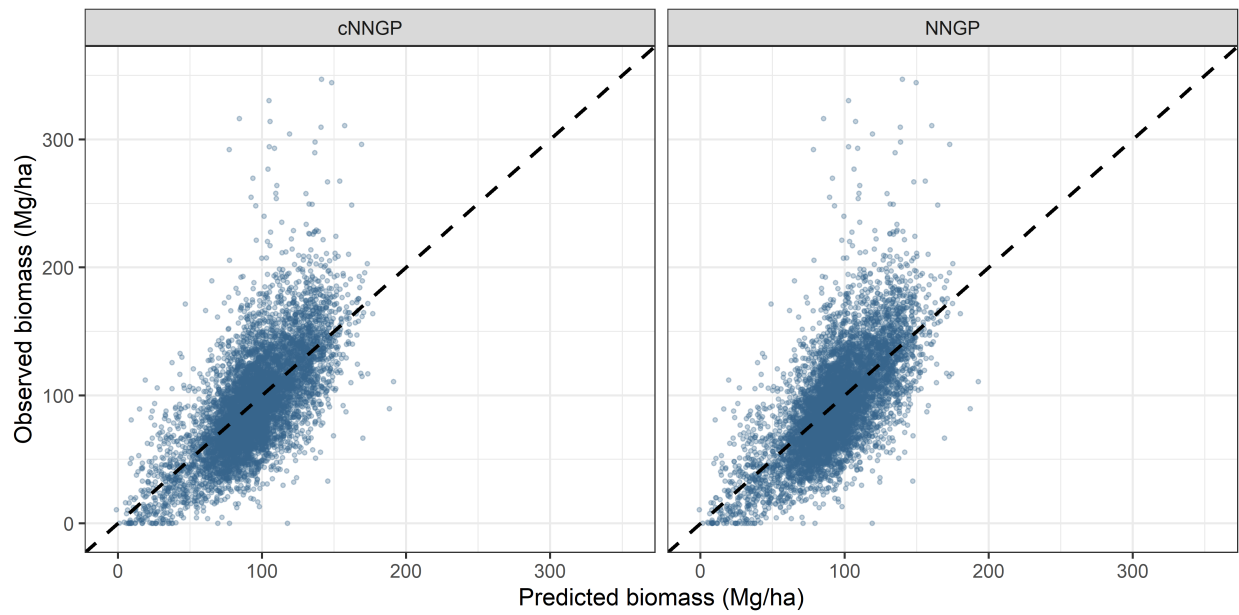


Figure A5: Observed versus predicted biomass from holdout data for each model.